ACS Catalysis

Research Article

pubs.acs.org/acscatalysis

Porphyrin-Metalation-Mediated Tuning of Photoredox Catalytic Properties in Metal–Organic Frameworks

Jacob A. Johnson,[†] Jian Luo,[†] Xu Zhang,[†] Yu-Sheng Chen,[‡] Martha D. Morton,[†] Elena Echeverría,[#] Fernand E. Torres,[#] and Jian Zhang*[,†]

[†]Department of Chemistry, University of Nebraska-Lincoln, Lincoln, Nebraska 68588-0304, United States

[‡]ChemMatCARS, Center for Advanced Radiation Sources, The University of Chicago, 9700 South Cass Avenue, Argonne, Illinois 60439, United States

[#]Department of Physics and Astronomy, Theodore Jorgensen Hall, 855 N 16th St., University of Nebraska, Lincoln, Nebraska 68588-0299, United States

Supporting Information

ABSTRACT: Photoredox catalytic activation of organic molecules via single-electron transfer processes has proven to be a mild and efficient synthetic methodology. However, the heavy reliance on expensive ruthenium and iridium complexes limits their applications for scale-up synthesis. To this end, photoactive metal–organic frameworks (MOFs) exhibit unique advantages as novel heterogeneous photocatalytic systems, yet their utilization toward organic transformations has been limited. Here we describe the preparation and synthetic applications of four isostructural porphyrinic MOFs, namely, UNLPF-10a, -10b, -11, and -12, which are composed of free base, In^{III}-, $Sn^{IV}Cl_2$-, and Sn^{IV}-porphyrin building blocks, respectively. We demonstrate that the metalation with high valent metal cations (In^{III} and Sn^{IV}) significantly modifies the electronic structure of porphyrin macrocycle and provides a highly oxidative photoexcited state that can undergo efficient reductive quenching processes to facilitate organic reactions. In particular, UNLPF-12 exhibits both outstanding photostability and efficient photocatalytic activities toward a range of important organic transformations including aerobic hydroxylation of arylboronic acids, amine coupling, and the Mannich reaction.

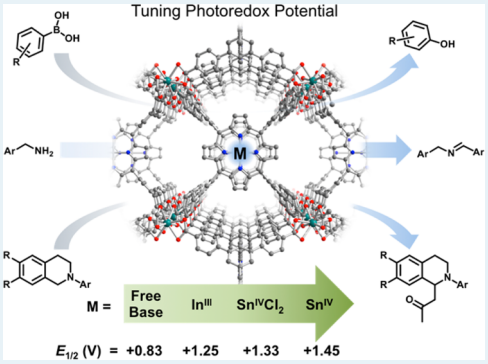

KEYWORDS: *metal–organic frameworks, photocatalysis, microporous materials, porphyrins, metalation*

INTRODUCTION

Visible-light photoredox catalysis allows for the use of solar-energy-generated photochemical potential to produce value-added organic compounds in a sustainable fashion.[1] This process is based upon the single-electron transfer (SET) events between organic substrates and photoredox catalysts that are typically transition metal complexes (e.g., $[Ru(bpy)_3]^{2+}$ (bpy =2,2′-bipyridine) and $Ir(ppy)_3$ (ppy =2-phenylpyridine)), and it has recently realized many complicated organic transformations.[2] However, Ru- and Ir- complexes are expensive, potentially toxic, and difficult to recycle. To this end, metal–organic frameworks (MOFs) represent an ideal heterogeneous photocatalytic platform to reduce the cost especially for scale-up synthesis.[3] MOFs are a class of porous crystalline solids that are constructed from the self-assembly of inorganic metal ions or clusters with organic ligands.[4] The remarkably tunable pore sizes and large surface areas of MOFs have rendered their wide array of applications in gas storage,[5] small molecule separation,[6] optics,[7] chemical sensing and imaging,[8] drug delivery and therapy,[9] among others. In particular, MOFs comprising large open channels can facilitate the diffusion of substrates and products and offer a unique advantage for their use as single-site solid catalysts and photocatalysts.[10] Indeed, over the past several years, a few photoactive MOFs have been prepared for inorganic reactions such as visible-light driven hydrogen evolution[11] and CO_2 reduction.[12]

Using MOFs for visible-light promoted organic transformations, however, has made much less progress. This is probably because most of the photoactive MOFs reported to date are based on the LMCT (ligand-to-metal charge transfer) transitions, which normally have limited, often not readily tunable visible light absorption.[13] More importantly, the large thermodynamic driving force and small kinetic barrier associated with LMCT usually lead to poor photon energy utilization. Thus, this type of photoactive MOF is mostly used for oxidative dye degradation[14] and generally shows inferior activities toward useful organic transformations.[15] A more robust and efficient strategy to construct photoactive MOFs for sophisticated organic transformations is to employ linkers that are functionalized with organic and metal–organic chromo-

Received: May 5, 2015
Revised: July 29, 2015
Published: August 3, 2015

DOI: 10.1021/acscatal.5b00941
ACS Catal. 2015, 5, 5283–5291

Scheme 1. Synthesis of Porphyrinic MOFs

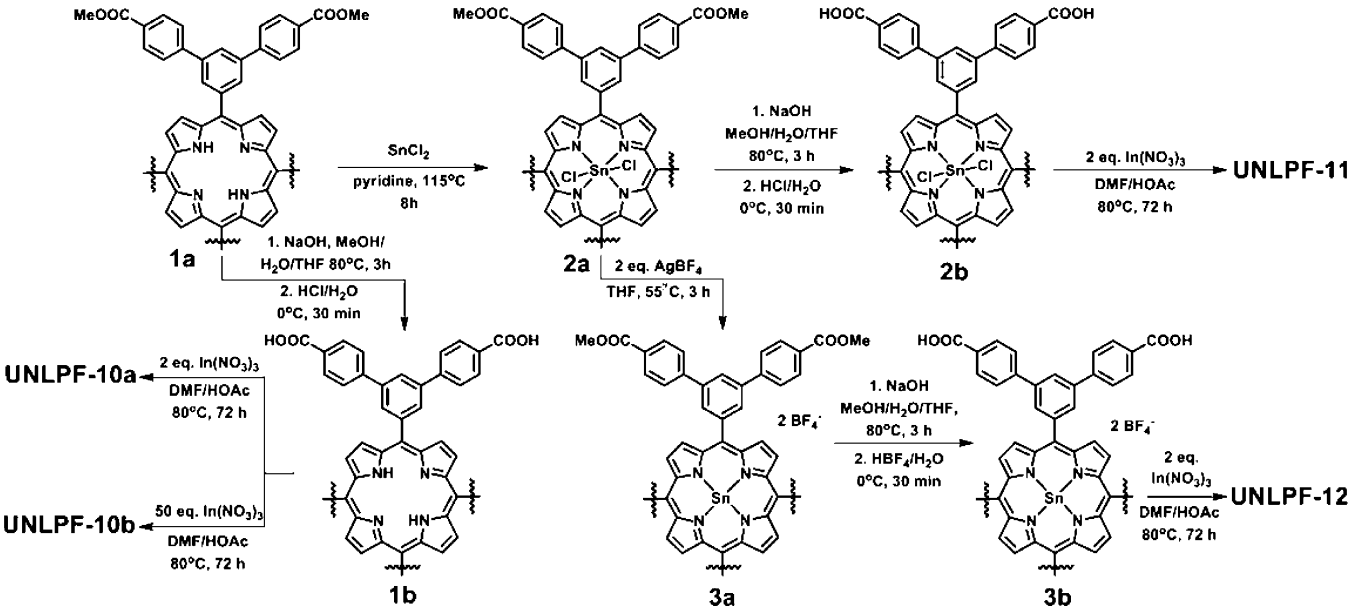

phores with well-known photocatalytic activities.[16] For instance, using linkers based on Ir- and Ru-complexes, Lin et al. constructed a series of UiO-67 MOFs that exhibit efficient activities toward aza-Henry reactions, aerobic amine coupling, and photo-oxidation of thioanisole.[17] Recently, Duan et al. successfully utilized MOFs consisting of triphenylamine photoredox moieties for α-alkylation of aldehydes with good enantioselectivity.[18]

Porphyrins and metalloporphyrins are common chromophores that can efficiently engage energy and/or electron transfer processes.[19] Thus, photoactive porphyrinic MOFs[20] can then be used for heterogeneous photocatalysis. Indeed, their utility in photocatalytic oxidation of thioanisole[21] and hydrogen evolution reaction[22] has been recently demonstrated. One unique yet underexplored feature of porphyrinic MOFs is the high dependence of their photophysical and photochemical properties on the coordinated metal ions, which can be easily modulated via the metalation of porphyrin macrocycle. We recently reported an indium porphyrinic MOF, UNLPF-10 (UNLPF: University of Nebraska–Lincoln porous framework), with adjustable photocatalytic activity via simple in situ porphyrin metalation.[21b] By changing the In^{III}/ligand ratio in the solvothermal synthesis, we systematically increased the extent of In^{III}–porphyrin moieties in UNLPF-10. Correspondingly, the photocatalytic activity of UNLPF-10 toward aerobic oxygenation of organic sulfides was enhanced because In^{III}–porphyrin is a more efficient singlet oxygen sensitizer compared to the free-base porphyrin.[21b] Additionally, it is known that coordinated metal ions can also significantly affect the photoredox properties of the porphyrin macrocycles. Herein, we report the use of metalation to fine-tune the photoredox catalytic activities of porphyrinic MOFs. Specifically, using UNLPF-10 as the prototypic structural motif, we synthesized and systematically characterized the photophysical and electrochemical properties of four isostructural porphyrinic MOFs, namely, UNLPF-10a, -10b, -11, and -12, which are composed of free base, In^{III}-, $Sn^{IV}Cl_2$-, and Sn^{IV}-porphyrin building blocks, respectively. We found that UNLPF-12, which is composed of coordinatively unsaturated high-valent metal centers (Sn^{IV}), exhibits the strongest oxidative capability and the highest efficiency in promoting the hydroxylation of arylboronic acids, aerobic amine coupling, and the Mannich reaction.

RESULTS AND DISCUSSION

Synthesis and Characterization. *Porphyrin Ligands.* The octatopic porphyrin ligand, tetrakis 3,5-bis((4-hydroxycarbonyl)-phenyl)phenylporphine (H_2L, **1b**) was synthesized using acid-mediated deprotection from its corresponding methyl ester (**1a**) according to our previously reported procedure (Scheme 1).[20g] The reaction of **1a** with $SnCl_2$ in pyridine under air yielded the $Sn^{IV}Cl_2$-metalated ester **2a**. To remove the two coordinated Cl^-, we employed an anion metathesis procedure[23] by reacting **2a** with 2 equiv of $AgBF_4$ in THF under argon which generated ester **3a**. The coordination environment of Sn^{IV} in **2a** and **3a** was confirmed by ^{119}Sn NMR: the chemical shift of ^{119}Sn in **2a** (δ = −588.4 ppm) appears higher than that in **3a** (δ = −620.1 ppm), which matches well with their structural analogues such as $Sn^{IV}Cl_2TPP$ (TPP^{2-} = *meso*-tetraphenylporphyrinate) (δ = −588.5 ppm) and $[Sn^{IV}TPP](BF_4)_2$ (δ = −619.9 ppm) (see Supporting Information for detailed synthetic procedure and Figure S1 for ^{119}Sn NMR spectra). In general, stronger axial ligands such as chloride can cause a downfield shift of ^{119}Sn in Sn^{IV}-porphyrins, possibly due to the effect of deshielding.[24] Further deprotection of **2a** by HCl and **3a** by HBF_4 yielded the octatopic ligand $Sn^{IV}Cl_2L$ (**2b**) and $[Sn^{IV}L](BF_4)_2$ (**3b**), respectively. The presence of the two BF_4^- in **3b** was confirmed by ^{19}F NMR using $AgBF_4$ as an internal standard (Figure S2).

UNLPF-10a and -10b. Two UNLPF-10 samples, UNLPF-10a and -10b, which contain ∼0% and ∼100% In^{III}-porphyrin moieties, respectively, were prepared via a solvothermal reaction of $In(NO_3)_3{\cdot}H_2O$ and **1b** in a *N*,*N*-dimethylformamide (DMF)/acetic acid mixture using In^{III}/ligand ratios of 2:1 and 50:1, respectively (see Supporting Information for detailed procedures). Note that a high In^{III}/ligand ratio (50:1) is essential here to achieve a complete In^{III}-metalation in UNLPF-10b.

UNLPF-11 and -12. UNLPF-11 and -12 were synthesized as dark red octahedral crystals (Figure S3) by a similar reaction of

DOI: 10.1021/acscatal.5b00941
ACS Catal. 2015, 5, 5283−5291

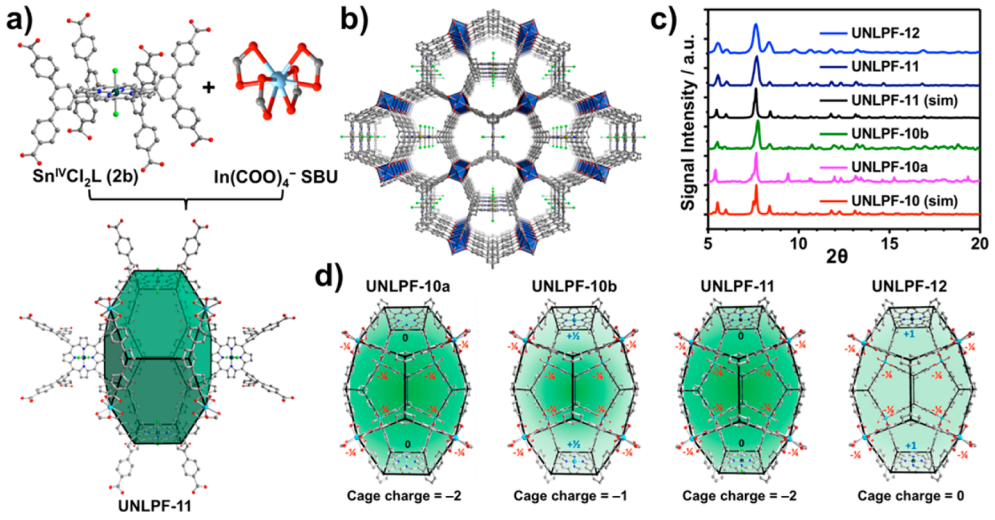

Figure 1. (a) Illustration of the octatopic ligand $Sn^{IV}Cl_2L$ and $[In(COO)_4]^-$ SBU forming the Williams β-tetrakaidecahedral cage in UNLPF-11. (b) Crystal structure of UNLPF-11 showing the one-dimensional channel along crystallographic *c* axis. (c) Simulated and experimental powder X-ray diffraction patterns. (d) Controlling the charge density of UNLPF-10a, -10b, -11, and -12 via metalation of porphyrins (charges are shown with respect to cage occupancy in the overall framework).

$In(NO_3)_3{\cdot}H_2O$ with $Sn^{IV}Cl_2L$ (**2b**) and $[Sn^{IV}L](BF_4)_2$ (**3b**), respectively (see Supporting Information for detailed procedures). Notably, the synthesis of UNLPF-11 and -12 is highly sensitive to the In^{III}/ligand ratio: 2 equiv of $In(NO_3)_3{\cdot}H_2O$ are required to achieve a good product yield and crystallinity. ^1H NMR spectra of the acid digested samples of UNLPF-11 and -12 confirm that all porphyrin moieties are coordinated with Sn^{IV} and the possible demetalation or metal ion exchange during the solvothermal synthesis does not occur (Supporting Information, Figure S4). It should be noted that BF_4^- is not present within the framework of UNLPF-12: no signal of ^{19}F was observed in the ^{19}F NMR spectrum of an acid-digested sample of UNLPF-12 (Figure S5). Presumably, BF_4^- remains in the original mother liquor in the solvothermal synthesis: the ^{19}F NMR spectrum indeed revealed a strong signal that can be attributed to $[Me_2NH_2]BF_4$ (Figure S5).

Single-crystal X-ray structural analysis reveals UNLPF-11 crystallizes in the orthorhombic space group *Pnnm* and is isostructural to UNLPF-10.[21b] Overall, the framework can be viewed as the close packing of 14-faced Williams β-tetrakaidecahedral cages.[21b,25] Each cage is composed of six $Sn^{IV}Cl_2L$ ligands and eight $[In(COO)_4]^-$ SBUs (secondary building units) (Figure 1a), and is enclosed by two square faces (two porphyrin planes), eight pentagonal faces (formed by perpendicularly oriented $Sn^{IV}Cl_2L$ ligands), and four hexagonal faces (formed by parallelly oriented $Sn^{IV}Cl_2L$ ligands). Notably, pentagonal shaped one-dimensional channels (1.1 Å × 1.1 Å) along the *c*-axis are beneficial for efficient mass transport, a good attribute for catalysis (Figure 1b). The phase purity of UNLPF-11 is confirmed by the powder X-ray diffraction pattern of a bulk sample, which matches well with the simulated pattern (Figure 1c). Likewise, the powder X-ray diffraction pattern of UNLPF-12 is also in good accordance to the simulated pattern (Figure 1c), indicating the isostructural nature. Additionally, X-ray photoemission spectroscopy (XPS) confirmed the presence of Sn^{IV} in UNLPF-12 with binding energies of 485.6 eV ($3d_{5/2}$) and 494.2 eV ($3d_{3/2}$) (Figure S7a).

We have previously shown that the presence of $[In(COO)_4]^-$ SBUs renders UNLPF-10 an anionically charged framework with encapsulated mobile counter cations ($Me_2NH_2^+$).[26] Moreover, the overall framework charge density is tunable by controlling the extent of In^{III}-metalation. Because the In^{III}-porphyrin moiety exhibits a "+1" charge, the effective charge density per cage in UNLPF-10a and UNLPF-10b are "−2" and "−1", respectively (Figure 1d). Similarly, in UNLPF-11, the porphyrin metal center $Sn^{IV}Cl_2$ gives way to a charge-neutral macrocycle, and thus, the effective charge density per cage is "−2" (Figure 1d). Accordingly, the "+2" charged Sn^{IV}-porphyrin centers in UNLPF-12 results in a net neutral framework (Figure 1d). Indeed, dye adsorption experiments confirmed the predicted charge densities. UNLPF-10a, -10b, and -11 adsorb approximately 2, 1, and 2 equiv of cationic methylene blue within 24 h, respectively, and do not adsorb the anionic dye, acid orange 7 (Supporting Information, Figure S8a–c). Conversely, the charge-neutral UNLPF-12 shows minimal adsorption for either the cationic or anionic dye (Figure S8d).

Spectroscopic and Electrochemical Characterization. The UV–vis absorption and fluorescence emission spectra of UNLPF-10a, -10b, -11, and -12 were measured and depicted in Figure 2. In order to make proper peak assignments, we also synthesized and measured the absorption and fluorescence emission spectra of H_2TPP (*meso*-tetraphenylporphyrin) and its metal complexes including InClTPP,[27] In(OAc)TPP,[28] $SnCl_2TPP$,[29] and $[SnTPP](BF_4)_2$[23a] as the model compounds (Supporting Information, Figures S9 and S10). The absorption spectrum of UNLPF-10a (Figure 2a and Table 1) shows similar features as that of H_2TPP (Figure S9), including a Soret band (B(0,0), 416 nm) and four Q bands in the visible region corresponding to π–π^* transitions: $Q_y(1,0)$, 519 nm; $Q_y(0,0)$, 562 nm; $Q_x(1,0)$, 596 nm; and $Q_x(0,0)$, 641 nm. The electronic absorption spectra of UNLPF-10b, -11, and -12 (Figure 2b–d and Table 1) display broad Soret bands (B(0,0)) with peak maxima around 430 nm and two weaker, less well-defined Q bands near 560 and 600 nm, respectively. On the basis of the absorption spectra of their model compounds (Figure S9), we assign the higher energy Q-band as the Q(1,0) transition (Table 1): the peak positions of Q(1,0) band are at 560, 565, and 556 nm when porphyrin macrocycle is coordinated to In^{III}, $[Sn^{IV}Cl_2]$, and Sn^{IV}, respectively. It is noted that the

DOI: 10.1021/acscatal.5b00941
ACS Catal. 2015, 5, 5283–5291

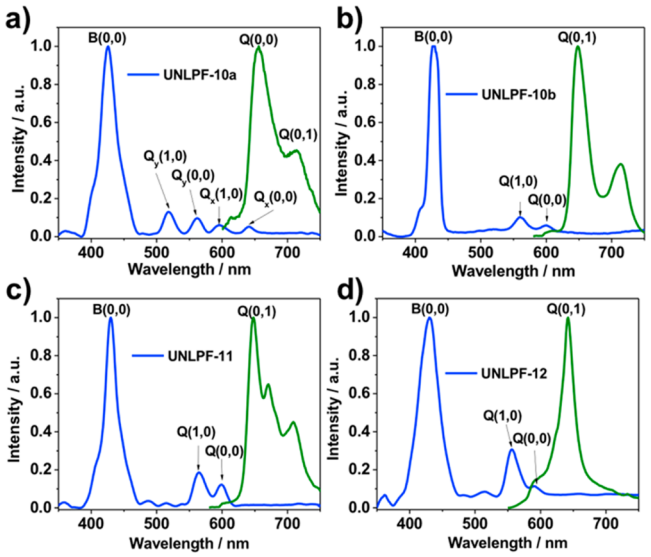

Figure 2. Steady-state electronic UV−vis absorption (blue) and fluorescence emission (green) spectra for UNLPF-10a (a), -10b (b), -11 (c), and -12 (d).

coordination of Cl^- in $[Sn^{IV}Cl_2]$ causes a small red shift (~270 cm^{-1}) of Q(1,0) band in both model compounds ($SnCl_2TPP$ and $[SnTPP](BF_4)_2$) and MOFs (UNLPF-11 and UNLPF-12) (Figure 2c,d and Table 1), consistent with previous observations.[30] Similarly, according to the fluorescence emission spectra obtained from model compounds, the emission peak around 650 nm is assigned as Q(0,0) for UNLPF-10a and Q(0,1) for UNLPF-10b, -11, and -12.[31] On the basis of these spectroscopic analyses, we were able to estimate the relevant zero−zero vibrational state excitation energy (E^{0-0}) for UNLPF-10a (1.91 V, intercept of the normalized absorption and emission of Q(0,0) state) and for UNLPF-10b, -11, and -12 (2.05, 2.04, and 2.07 V, respectively, medium wavelengths between corresponding absorbance Q(1,0) and emission Q(0,1) state) (Table 1).

Cyclic-voltammetry was used to determine the ground-state oxidation and reduction potentials for model compounds as well as four porphyrinic MOFs. The measured reduction and oxidation couples of H_2TPP,[32] InClTPP,[33] In(OAc)TPP,[34] and $SnCl_2TPP$[35] were consistent with previously reported values (Table 1 and Supporting Information, Figure S11). Briefly, all model compounds undergo two reversible single-electron reductions and two reversible single-electron oxidations, which are porphyrin-centered. Notably, the $E_{1/2}(M/M^-)$ (describing the half-reaction $M + e^- \rightarrow M^-$) for all four metalated porphyrins are less negative compared to that of H_2TPP (Table 1). Moreover, as the valence of the coordinated metal ion increases from 3+ to 4+, the $E_{1/2}(M/M^-)$ anodically shifts from −1.06/−1.07 V ($In^{III}ClTPP/In^{III}(OAc)TPP$) to −0.80/−0.76 V ($Sn^{IV}Cl_2TPP/[Sn^{IV}TPP](BF_4)_2$). Likewise, the $E_{1/2}(M^+/M)$ anodically shifts from +1.21/+1.16 V ($In^{III}ClTPP/In^{III}(OAc)TPP$) to +1.43/+1.44 V ($Sn^{IV}Cl_2TPP/[Sn^{IV}TPP](BF_4)_2$). Combining the spectroscopic and electrochemical data, the excited-state reduction potentials, $E_{1/2}(M^+/*M)$ (describing the half-reaction $M^+ + e^- \rightarrow *M$, "*" denotes the excited state) and $E_{1/2}$ ($*M/M^-$) (describing the half-reaction $*M + e^- \rightarrow M^-$) of the model compounds, have been estimated (Table 1). It is clear that the strong electron-withdrawing effect induced by high valent metal cations on the porphyrin ring stabilizes both HOMO (highest occupied molecular orbital) and LUMO (the lowest unoccupied molecular orbital) energy levels, leading to the reduction of porphyrin macrocycle occurring at a less-negative potential. Accordingly, the photoexcited porphyrin is transformed from the weakly oxidative H_2TPP ($E_{1/2}(M*/M^-)$ = +0.68 V) to moderately oxidative InClTPP/In(OAc)TPP ($E_{1/2}(*M/M^-)$ = +0.98/+0.97 V), and to strongly oxidative $SnCl_2TPP/[SnTPP](BF_4)_2$ ($E_{1/2}(*M/M^-)$ = +1.23/+1.30 V).

Cyclic voltammograms of the four porphyrinic MOFs exhibit weaker reduction current and only the $E_{1/2}(M/M^-)$ were detectable and appeared less negative compared to those of their corresponding model compounds (Supporting Information, Figure S12): the anodic shifts are 0.09 V in UNLPF-10a, ~ 0.26 V in UNLPF-10b, and ~0.10 V in UNLPF-11 and -12. We tentatively attribute the observed anodic shift to the slight change in electronic structure of the porphyrin ligand upon MOF formation, not the difference in substituents on porphyrin macrocycle. Indeed, H_2TPP and its derivative **1a** exhibit essentially the same spectroscopic and electrochemical properties (Table 1 and Figure S9−11). The $E_{1/2}$ ($*M/M^-$) of four porphyrinic MOFs were calculated to be +0.79 V, +1.25 V,

Table 1. Photophysical and Electrochemical Parameters of Porphyrinic MOFs and Their Model Compounds

	absorption (nm)[a]			emission (nm)[a]						
photocatalyst	B(0,0)	Q(1,0)	Q(0,0)	Q(0,0)	Q(0,1)	E^{0-0} (eV)	$E_{1/2}(M/M^-)$ (V)[c]	$E_{1/2}(M^+/M)$ (V)[c]	$E_{1/2}(M^+/*M)$ (V)[c,d]	$E_{1/2}(*M/M^-)$ (V)[c,e]
H_2TPP	416	514[b] 590[b]	547[b] 649[b]	656	714	1.90	−1.22	+1.01	−0.89	+0.68
InClTPP	423	557	597	609	657	2.04	−1.06	+1.21	−0.83	+0.98
In(OAc)TPP	423	558	598	606	655	2.04	−1.07	+1.16	−0.88	+0.97
$SnCl_2TPP$	426	560	600	617	659	2.03	−0.80	+1.43	−0.60	+1.23
$[SnTPP](BF_4)_2$	417	552	590	603	651	2.06	−0.76	+1.44	−0.62	+1.30
1a	421	516[b] 588[b]	550[b] 647[b]	655	705	1.90	−1.23	+1.02	−0.88	+0.67
UNLPF-10a	426	519[b] 596[b]	562[b] 641[b]	656	714	1.91	−1.08	-	-	+0.83
UNLPF-10b	429	560	600	606	648	2.05	−0.80	-	-	+1.25
UNLPF-11	430	565	598	607	648	2.04	−0.71	-	-	+1.33
UNLPF-12	431	556	591	593	642	2.07	−0.65	-	-	+1.42

[a]In this notation, the numbers in parentheses are number of vibrational quanta in the excited and ground states, respectively. [b]Split due to the reduced symmetry of free base porphyrins compared to their metalated counterparts. [c]$E_{1/2}(M^+/*M)$, $E_{1/2}(*M/M^-)$, $E_{1/2}(M^+/M)$, and $E_{1/2}(M/M^-)$ describe half-reactions $M^+ + e^- \rightarrow *M$, $*M + e^- \rightarrow M^-$, $M^+ + e^- \rightarrow M$, and $M + e^- \rightarrow M^-$, respectively. [d]$E_{1/2}(M^+/*M) = E^{0-0} - E_{1/2}(M^+/M)$. [e]$E_{1/2}(*M/M^-) = E^{0-0} - E_{1/2}(M/M^-)$.

DOI: 10.1021/acscatal.5b00941
ACS Catal. 2015, 5, 5283−5291

+1.33 V, and +1.42 V for UNLPF-10a, -10b, -11, and -12, respectively (Table 1). Compared to their model compounds, porphyrinic MOFs are slightly more oxidative. In particular, with fairly positive $E_{1/2}$ (*M/M$^-$) values (+1.25−1.42 V), UNLPF-11b, -11, and -12 are expected to exhibit excellent activity in promoting organic reactions via a reductive quenching pathway, where the excited state of the porphyrinic MOF induces the oxidation of an electron donor. Here, we set out to test the activities of porphyrinic MOFs in three representative photoredox catalytic organic transformations, where an alkylamine is used as either a sacrificial electron donor or an electron-rich substrate to initialize the photoredox catalytic processes.

Oxidative Hydroxylation of Arylboronic Acids. We first used the aerobic oxidative hydroxylation of arylboronic acids[36] to evaluate the photocatalytic activities of porphyrinic MOFs. According to the previously proposed reaction mechanism (Scheme 2),[36] the excited photocatalyst first obtains an electron

Scheme 2. Proposed Mechanism for the Photocatalytic Oxidative Hydroxylation of Arylboronic Acids

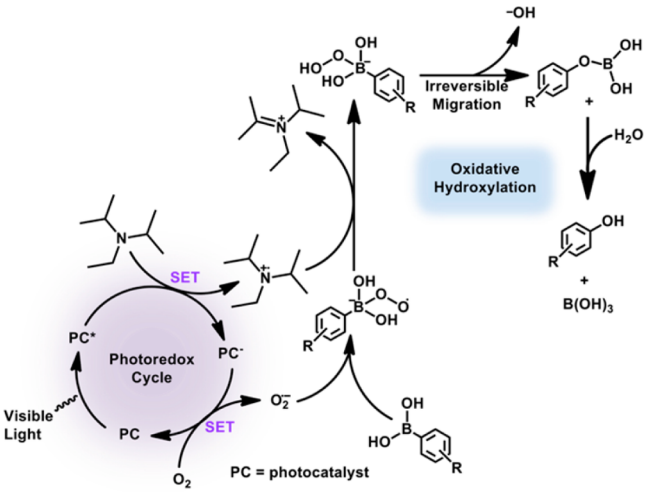

from a sacrificial electron donor (e.g., *N*,*N*-diisopropylethylamine, DIPEA) and then reduces O_2 in air to the superoxide radical anion ($O_2^{\bullet-}$).[36] Further, $O_2^{\bullet-}$ adds to the vacant *p*-orbital of boron leading to the subsequent 1,2-aryl shift and hydrolysis to produce the final phenolic product. Because the $E_{1/2}$(M$^+$/M) of DIPEA is +0.90 V vs SCE[37] and $E_{1/2}$(M/M$^-$) of O_2 is −0.86 V vs SCE (in DMF),[38] photocatalysts with an $E_{1/2}$(*M/M$^-$) higher than +0.90 V and $E_{1/2}$(M/M$^-$) lower than −0.86 V are expected to oxidize the amine and lead to the subsequent O_2 reduction.

We systematically examined the photocatalytic activities of four porphyrinic MOFs as well as their model compounds toward the hydroxylation of 4-formylbenzeneboronic acid (**4a**), which generates 4-formylphenol (**5a**) as the product (Table 2). It is found that the photocatalyst's efficiency is largely dictated by a thermodynamically favorable $E_{1/2}$(*M/M$^-$) for amine oxidation. For example, due to its weak oxidative capability toward DIPEA, H_2TPP gives essentially no conversion ($E_{1/2}$(*M/M$^-$) = +0.68 V vs SCE) (entry 1, Table 2). Conversely, both InClTPP and In(OAc)TPP finish the reaction within ∼24 h (entries 2 and 3, Table 2), consistent with their higher $E_{1/2}$ (*M/M$^-$) (∼+0.97 V vs SCE, Table 1). $SnCl_2$TPP and [SnTPP](BF$_4$)$_2$ with even stronger oxidative capabilities

Table 2. Screening Photocatalysts for Oxidative Hydroxylation of 4-Formylbenzeneboronic Acid[a]

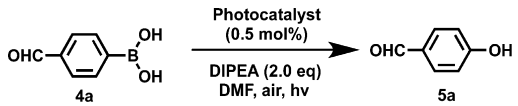

entry	photocatalyst	t (h)	% yield[b]
1	H_2TPP	24	trace
2	InClTPP	24	97
3	In(OAc)TPP	24	94
4	$SnCl_2$TPP	12	96
5	[SnTPP](BF$_4$)$_2$	10	> 99
6	UNLPF-10a	24	87
7	UNLPF-10b	4	> 99
8	UNLPF-11	3.5	> 99
9	UNLPF-12	2.5	> 99
10[c]	UNLPF-12	2.5	95
11[d]	UNLPF-12	24	n.r.
12[e]	UNLPF-12	24	trace
13[f]	UNLPF-12	24	trace

[a]Reaction condition: photocatalyst (0.5 μmol, 0.5 mol % based on porphyrin moiety), **4a** (0.1 mmol), DIPEA (0.2 mmol), 1.0 mL dry DMF, 14 W CFL (distance ≈8 cm). [b]Determined by ^{1}H NMR. [c]After 4th recycle. [d]No photocatalyst. [e]No light. [f]Ar atmosphere.

($E_{1/2}$ (*M/M$^-$) = +1.23/+1.30 V vs SCE, Table 1) exhibit the highest efficiency among all model compounds, finishing the reaction within only 12 h (entries 4 and 5, Table 2). Surprisingly, porphyrinic MOFs exhibit significantly higher efficiencies than their model compounds. For example, compared to the inactive H_2TPP, UNLPF-10a gives an 87% conversion after 24 h (entry 6, Table 2), which can be attributed to its slightly more positive $E_{1/2}$(*M/M$^-$) of +0.83 V compared to that of H_2TPP (Table 1). UNLPF-10b and -11 exhibit even faster reaction rates, finishing the hydroxylation within 4 and 3.5 h, respectively (entries 7 and 8, Table 2). More remarkably, UNLPF-12 reaches a full conversion within 2.5 h with a 92% isolated yield (entry 9, Table 2) despite its inadequate $E_{1/2}$(M$^+$/M) (−0.65 V vs SCE) to reduce O_2. Therefore, the oxidation of the amine has a greater effect on the overall reaction rate compared to the reduction of O_2, which is reasonable considering the amine's higher concentration (∼0.2 M) versus that of O_2 (∼1.31 mM in DMF).[39] Indeed, the formation of $O_2^{\bullet-}$ in the presence of DIPEA was confirmed via EPR (electron paramagnetic resonance) spectroscopy by employing the superoxide radical trapping agent DMPO (5,5-dimethyl-1-pyrroline *N*-oxide) (Figure S17).

However, a favorable photoredox potential alone cannot explain the dramatic difference in reaction rates between model compounds with MOFs. In fact, the slower reaction rate of model compounds is largely due to inferior photostability and severe decomposition under the reaction conditions. We observed a significant color change following the hydroxylation of **4a**. Indeed, UV−vis absorption spectroscopy indicates a significant amount (>80%) of [SnTPP](BF$_4$)$_2$ decomposed after the reaction and new species that absorb at approximately 620 and 510 nm formed (Figure 3a). Further reuse of [SnTPP](BF$_4$)$_2$ for a second time only gave a 12% yield (Supporting Information, Figure S15). In contrast, UNLPF-12 exhibits no sign of deactivation even after five times of repeated reaction (entry 10, Table 2). The UV−vis spectrum (Figure 3b) and powder X-ray diffraction pattern (Figure S16) of

DOI: 10.1021/acscatal.5b00941
ACS Catal. 2015, 5, 5283−5291

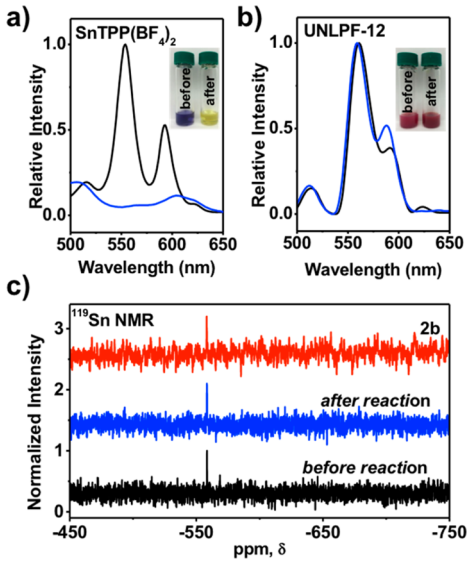

Figure 3. UV−vis absorption spectra of reaction mixtures of **4a**, DIPEA, and $[SnTPP](BF_4)_2$ (a) and UNLPF-12 (b) in DMF before (black) and after (blue) photooxidative hydroxylation and respective photographs (insets). (c) ^{119}Sn NMR spectra for acid (DCl:d_6-DMSO, v/v = 1:6) digested samples of UNLPF-12 before (black) and after (blue) photooxidative hydroxylation of **4a**. Note that Cl^- easily binds to the UNLPF-12 Sn-porphyrin centers in the presence of DCl, as indicated by the similar ^{119}Sn chemical shift of ligand **2b** (red).

UNLPF-12 after reuse exhibits no significant structural change, also indicating its outstanding resistance to deactivation. It should be noted that the coordination environment and oxidation state of Sn^{IV} porphyrin metal center are preserved during the reaction as indicated by the XPS spectra (Figure S7c and Table S2) and ^{119}Sn NMR (Figure 3c) for a sample of UNLPF-12 before and after photooxidative hydroxylation of **4a**.

Control experiments (entries 11−13, Table 2) confirmed the essential role of the photocatalyst, light, and oxygen in this reaction. Due to its outstanding performance, we chose UNLPF-12 as the prototypic photocatalyst to study the reaction scope (Table 3). Arylboronic acids bearing electron-withdrawing (entries 1−7, Table 3) and electron-donating (entries 8−11, Table 3) substituents can all be smoothly converted into the corresponding aryl alcohols in good to excellent yields (83−96%) within 2−10 h. Generally, the reaction proceeds faster for electron-deficient arylboronic acids due to greater accessibility of the vacant boron *p*-orbital. Notably, UNLPF-12 is more efficient than common transition metal complex photocatalysts including $[Ru(bpy)_3]^{2+}$ in promoting the hydroxylation of 4-formylbenzeneboronic acid (entries 13−15, Table 3).[36a]

Oxidative Amine Coupling. We next tested the activities of MOF-based photocatalysts in the aerobic oxidation of primary amines to yield imines, a widely studied model reaction.[40] According to the typical electron-transfer-based mechanism (Figure 4a),[41] the excited photocatalyst first oxidizes the amine to generate a cationic amine radical and then reduces molecular oxygen to $O_2^{\bullet-}$. The subsequent reaction between the amine radical and $O_2^{\bullet-}$ yields the imine intermediate, which undergoes a nucleophilic addition with a second primary amine to give the coupled imine product (Figure 4a). Here, benzylamine (**6a**) was used to optimize the coupling reaction condition. First, the photocatalyst, light irradiation, and air were found to be essential components for

Table 3. Photocatalytic Oxidative Hydroxylation of Arylboronic Acids[a]

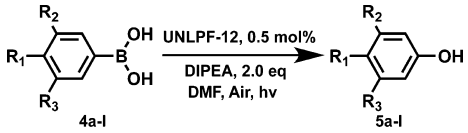

entry	R_1	R_2	R_3	product	t (h)	% yield[b]
1	CHO	H	H	**5a**	2.5	> 99 (92)
2	H	CHO	H	**5b**	3.5	95 (94)
3	CN	H	H	**5c**	2.0	96 (89)
4	CO_2Me	H	H	**5d**	2.5	> 99 (96)
5	$B(OH)_2$	H	H	**5e**	6	95 (87)
6	Cl	H	H	**5f**	4	98 (95)
7	H	Cl	H	**5g**	3.5	97 (95)
8	Me	H	H	**5h**	6	94 (88)
9	H	Me	H	**5i**	6	95 (93)
10	H	Me	Me	**5j**	10	88 (83)
11	MeO	H	H	**5k**	8	93 (90)
12	Ph	H	H	**5l**	6	96 (95)
13[c]	CHO	H	H	**5a**	2.5	21
14[d]	CHO	H	H	**5a**	2.5	65
15[e]	CHO	H	H	**5a**	2.5	62

[a]Reaction condition: UNLPF-12 (0.5 μmol, 0.5 mol % based on porphyrin moiety), **4** (0.1 mmol), DIPEA (0.2 mmol), 2.5 mL dry DMF, 14 W CFL (distance ≈8 cm). [b]Isolated yields in parentheses. [c]$[Ru(bpy)_3]^{2+}$ used as catalyst. [d]$[Ir[dF(CF_3)ppy]_2(dtbbpy)]^+$ used as catalyst (dF(CF_3)ppy = 2-(2,4-difluorophenyl)-5-trifluoromethylpyridine, dtbbpy = 4,4′-di-*tert*-butyl-2,2′-bipyridine). [e]$[Ir[dF(CF_3)ppy]_2(bpy)]^+$ used as catalyst.

this transformation (entries 3−5, Table 4). From a thermodynamic perspective, UNLPF-10b, -11, and -12 are expected to exhibit a good photocatalytic activity for this reaction because their $E_{1/2}$ ($^*M/M^-$) is more positive than the $E_{1/2}$ (M^+/M) of benzylamine (~+1.23 V vs SCE, Figure S19). As expected, UNLPF-12 appears to be the most active photocatalyst among all porphyrinic MOFs studied. The reaction of benzylamine in the presence of UNLPF-12 (0.4 mol % based on Sn^{IV}-porphyrin) in CH_3CN exposed to air under irradiation with a 14 W white CFL results in imine **7a** in 99% yield after 2 h (entry 1, Table 4), which is faster that than UNLPF-11 (5.5 h) and UNLPF-10b (5 h) (entries 7 and 9, Table 4).

Interestingly, in spite of its inadequate $E_{1/2}$ ($^*M/M^-$) (+0.79 V vs SCE), UNLPF-10a also exhibits a good catalytic activity albeit with a slower reaction rate: a 99% conversion with 97% selectivity was achieved within 11.5 h (entry 11, Table 4). Therefore, the observed activity of UNLPF-10a should not be attributed, at least solely, to the electron transfer mechanism. In fact, an alternative mechanism based on the singlet oxygen ($^1O_2$) induced amine oxidation is also operable.[42] In this mechanism, a photosensitizer that can efficiently generate highly oxidative singlet oxygen ($^1O_2$) via energy transfer is necessary to form the essential phenylmethanimine intermediate (Figure 4a). Indeed, using EPR experiments where TEMP (2,2,6,6-tetramethylpiperidine) was employed as the trapping agent, we found that UNLPF-10a can efficiently generate $^1O_2$ (Supporting Information, Figure S21). Further, because the lifetime of $^1O_2$ is generally longer in deuterated solvents,[43] an increase of reaction rate in deuterated solvents compared to their protonated counterparts enhanced in the presence of UNLPF-10a (99%, 7.5 h) compared to in CH_3CN (99%, 11.5

DOI: 10.1021/acscatal.5b00941
ACS Catal. 2015, 5, 5283−5291

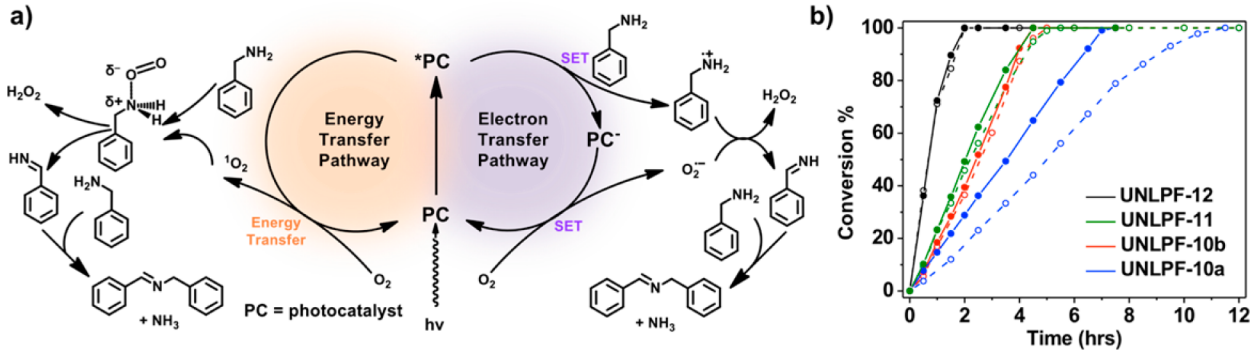

Figure 4. (a) Proposed mechanisms for the photocatalytic oxidative amine coupling reaction: singlet oxygen (energy transfer) and superoxide radical anion (electron transfer) pathways. (b) Plots of conversion of benzylamine versus time in oxidative amine coupling using porphyrinic MOFs as photocatalysts in CH_3CN (open circle) and CD_3CN (solid circle).

Table 4. Photocatalytic Oxidative Amine Coupling[a]

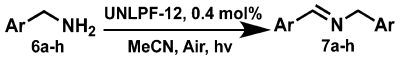

entry	aryl	product	t (h)	% yield[b]	% selectivity[b]
1	Ph	**7a**	2	> 99	> 99
2[c]	Ph	**7a**	2	>99	>99
3[d]	Ph	**7a**	24	trace	-
4[e]	Ph	**7a**	24	n.r.	-
5[f]	Ph	**7a**	24	n.r.	-
6[g]	Ph	**7a**	2	98	97
7[h]	Ph	**7a**	5.5	>99	>99
8[h,c]	Ph	**7a**	4.5	>99	>99
9[i]	Ph	**7a**	5	>99	99
10[i,c]	Ph	**7a**	4.5	>99	>99
11[j]	Ph	**7a**	11.5	>99	97
12[j,c]	Ph	**7a**	7.5	>99	99
13	4-F-Ph	**7b**	2	>99	99
14	4-Cl-Ph	**7c**	1.5	>99	99
15	4-Me-Ph	**7d**	3	>99	98
16	4-MeO-Ph	**7e**	4	>99	97
17	4-pyridinyl	**7f**	8	>99	91
18	2-furanyl	**7g**	10	88	99

[a]Reaction condition: UNLPF-12 (1.0 μmol, 0.4 mol % based on porphyrin moiety), **6** (0.27 mmol), 1 mL dry CH_3CN, 14 W CFL (distance ≈8 cm). [b]Determined by ^{1}H NMR, and the byproduct is the corresponding aryl aldehyde. [c]CD_3CN used as solvent. [d]No photocatalyst. [e]No light. [f]Ar atmosphere. [g]After 4th recycle. [h]UNLPF-11 used as catalyst. [i]UNLPF-10b used as catalyst. [j]UNLPF-10a used as catalyst.

h) (entries 11 and 12, Table 4 and Figure 4b). Conversely, no significant solvent effect for UNLPF-12, -11, and -10b was observed (entries 1, 2, 7−10, Table 4 and Figure 4b). This result indicates that for reactions catalyzed by UNLPF-12, -11, and -10b, the reaction primarily involves the photoinduced electron transfer pathway. It should be noted, however, that the electron transfer pathway cannot be completely ruled out for UNLPF-10a. Indeed, EPR spectra indicated that when DMPO was present in an aerated CH_3CN solution of benzylamine and UNLPF-10a, weak signals were observed upon light irradiation (Figure S22), which suggests UNLPF-10a is weakly capable of generating $O_2^{\bullet-}$ to initiate the amine coupling via photoredox reaction pathway.

The reaction scope was studied using UNLPF-12 as the photocatalyst. Photo-oxidative coupling of benzylamine and its derivatives generally proceed smoothly with high conversion (>88%) and high selectivity (>91%) (entries 13−16, Table 4). The substituent on the phenyl ring has an insignificant effect on the reaction rate and selectivity. Additionally, this photocatalytic system is tolerant to substrates containing heteroatoms (such as O, S, and N) on the aromatic ring (entries 17−19, Table 4) with only a small decrease in conversion, consistent with previous results where TiO_2 was used as the photocatalyst.[41a] Notably, the photocatalytic efficiency of UNLPF-12 for the coupling of primary amine **6a** is comparable to those promoted by common transition metal complexes (Supporting Information, Table S3). UNLPF-12 also exhibits excellent recyclability: no diminished conversion was observed after four times of reuse (entry 6, Table 4), and the recovered catalyst retained the crystalline integrity (Figure S20).

Aerobic Photooxidative Mannich Reaction. Lastly, to demonstrate their wider utility, we examined the catalytic activities of porphyrinic MOFs in the well-studied photooxidative Mannich reactions.[44] This dehydrogenation cross-coupling reaction involves the catalytic oxidation of α-amino C−H bonds to generate reactive iminium ions and subsequent C−C bond formation between the iminium ions and a carbon nucleophile. A typical Mannich reaction involves the irradiation of an aerated mixture containing photocatalyst, tertiary amine, acetone, and L-proline (to form the enamine nucleophile). An excellent conversion of 98% was achieved after 7 h when UNLPF-12 and **8a** was employed as the photoredox catalyst and tertiary amine, respectively; the reaction rate is again faster than those of the other three porphyrinic MOFs (entries 1−4, Table 5) and many common transition-metal complex photocatalysts (Supporting Information, Table S4). The photocatalyst, light, and air were confirmed to be integral to this transformation (entries 5−7, Table 5). UNLPF-12 also exhibits an excellent recyclability (entry 8, Table 5) without losing crystallinity (Figure S25). We also examined the reaction scope using UNLPF-12 as the photocatalyst under the optimized condition (entries 9−13, Table 5). In general, the cross-dehydrogenative coupling products with acetone were obtained in good to excellent yields (87−98%).

According to the proposed mechanism (Supporting Information, Scheme S2), photoexcited UNLPF-12 oxidizes a tertiary amine (e.g., **8a**) into a radical cation species and the reduced UNLPF-12 promotes the reduction of O_2 to $O_2^{\bullet-}$. The radical cation species is then deprotonated by $O_2^{\bullet-}$ to form the highly reactive iminium ion, which enters the organocatalytic cycle and reacts with the enamine nucleophile generated by L-proline-activated acetone to give the desired cross-coupling

DOI: 10.1021/acscatal.5b00941
ACS Catal. 2015, 5, 5283−5291

Table 5. Photocatalytic Oxidative Mannich Reaction[a]

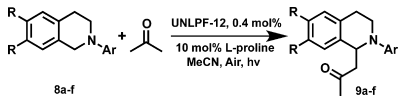

entry	R	Ar	product	t (h)	% yield[b]
1[c]	H	Ph	**9a**	48	83
2[d]	H	Ph	**9a**	15	92
3[e]	H	Ph	**9a**	12	97
4	H	Ph	**9a**	7	98
5[f]	H	Ph	**9a**	7	trace
6[g]	H	Ph	**9a**	7	trace
7[h]	H	Ph	**9a**	7	trace
8[i]	H	Ph	**9a**	7	96
9	H	4-Br-Ph	**9b**	7	98
10	H	4-MeO-Ph	**9c**	8	87
11	MeO	Ph	**9d**	7	96
12	MeO	4-Br-Ph	**9e**	8	95
13	MeO	4-MeO-Ph	**9f**	9	89

[a]Reaction condition: UNLPF-12 (1 μmol, 0.4 mol % based on porphyrin moiety), **8** (0.25 mmol), acetone (0.25 mmol), L-proline (0.025 mmol, 10 mol %), 6.0 mL dry CH_3CN, 14W CFL (distance ≈8 cm). [b]Determined by ^{1}H NMR with 2-bromoacetophenone as an internal standard. [c]UNLPF-10a used as catalyst. [d]UNLPF-10b used as catalyst. [e]UNLPF-11 used as catalyst. [f]No photocatalyst. [g]No light. [h]Ar atmosphere. [i]After 4th recycle.

product. The formation of $O_2^{\bullet-}$ was confirmed by EPR spectroscopy. UNLPF-12 alone was not able to generate $O_2^{\bullet-}$; however, in the presence of **8a**, DMPO, air, and UNLPF-12, a strong radical signal was observed, confirming the formation of $O_2^{\bullet-}$ under the reaction condition (Figure S24).

CONCLUSIONS

We have synthesized four isostructural porphyrinic MOFs and investigated their photoredox catalytic activities toward three representative organic transformations including aerobic hydroxylation of arylboronic acids, oxidative primary amine coupling, and the Mannich reaction. Compared to their molecular model compounds, porphyrinic MOF-based photocatalysts exhibit a considerably enhanced photostability and excellent recyclability. Most importantly, metalation with high-valent metal cations (In^{III} and Sn^{IV}) significantly modifies the electronic structure of the porphyrin and provides a highly oxidative photoexcited state that undergoes efficient reductive quenching processes to facilitate subsequent organic transformations. Porphyrin metalation indeed provides a convenient approach to fine-tune and optimize the photoredox catalytic activities of MOFs.

ASSOCIATED CONTENT

Supporting Information

The Supporting Information is available free of charge on the ACS Publications website at DOI: 10.1021/acscatal.5b00941.

Materials, general procedure, synthesis of UNLPF-11, -12, spectroscopic and electrochemical characterization, photocatalytic study (PDF)
Crystallographic data (CIF)

AUTHOR INFORMATION

Corresponding Author

*E-mail: jzhang3@unl.edu.

Notes

The authors declare no competing financial interest.

ACKNOWLEDGMENTS

The authors acknowledge the support from the University of Nebraska-Lincoln. This work is also partially supported by the donors of the American Chemical Society Petroleum Research Fund (53678-DNI10). Use of the X-ray photoemission spectrometer was supported by National Science Foundation through the Nebraska MRSEC (DMR-1420645). ChemMatCARS Sector 15 is principally supported by the Divisions of Chemistry (CHE) and Materials Research (DMR), National Science Foundation, under grant number NSF/CHE-1346572. Use of the Advanced Photon Source, an Office of Science User Facility operated for the U.S. Department of Energy (DOE) Office of Science by Argonne National Laboratory, was supported by the U.S. DOE under Contract No. DE-AC02-06CH11357.

REFERENCES

(1) (a) Ciamician, G. *Science* **1912**, *36*, 385−394. (b) Fagnoni, M.; Dondi, D.; Ravelli, D.; Albini, A. *Chem. Rev.* **2007**, *107*, 2725−2756. (c) Hoffmann, N. *Chem. Rev.* **2008**, *108*, 1052−1103. (d) Ravelli, D.; Fagnoni, M.; Albini, A. *Chem. Soc. Rev.* **2013**, *42*, 97−113.
(2) (a) Yoon, T. P.; Ischay, M. A.; Du, J. *Nat. Chem.* **2010**, *2*, 527−532. (b) Narayanam, J. M.; Stephenson, C. R. *Chem. Soc. Rev.* **2011**, *40*, 102−113. (c) Prier, C. K.; Rankic, D. A.; MacMillan, D. W. *Chem. Rev.* **2013**, *113*, 5322−5363. (d) Schultz, D. M.; Yoon, T. P. *Science* **2014**, *343*, 1239176.
(3) Zhang, T.; Lin, W. *Chem. Soc. Rev.* **2014**, *43*, 5982−5993.
(4) (a) Long, J. R.; Yaghi, O. M. *Chem. Soc. Rev.* **2009**, *38*, 1213−1214. (b) Zhou, H. C.; Long, J. R.; Yaghi, O. M. *Chem. Rev.* **2012**, *112*, 673−674. (c) Furukawa, H.; Cordova, K. E.; O'Keeffe, M.; Yaghi, O. M. *Science* **2013**, *341*, 1230444. (d) Wang, C.; Liu, D.; Lin, W. *J. Am. Chem. Soc.* **2013**, *135*, 13222−13234. (e) Foo, M. L.; Matsuda, R.; Kitagawa, S. *Chem. Mater.* **2014**, *26*, 310−322.
(5) (a) Suh, M. P.; Park, H. J.; Prasad, T. K.; Lim, D. W. *Chem. Rev.* **2012**, *112*, 782−835. (b) Sumida, K.; Rogow, D. L.; Mason, J. A.; McDonald, T. M.; Bloch, E. D.; Herm, Z. R.; Bae, T. H.; Long, J. R. *Chem. Rev.* **2012**, *112*, 724−781. (c) He, Y.; Zhou, W.; Qian, G.; Chen, B. *Chem. Soc. Rev.* **2014**, *43*, 5657−5678. (d) An, J.; Rosi, N. L. *J. Am. Chem. Soc.* **2010**, *132*, 5578−5579.
(6) Li, J. R.; Sculley, J.; Zhou, H. C. *Chem. Rev.* **2012**, *112*, 869−932.
(7) Wang, C.; Zhang, T.; Lin, W. *Chem. Rev.* **2012**, *112*, 1084−1104.
(8) (a) Della Rocca, J.; Lin, W. *Eur. J. Inorg. Chem.* **2010**, *2010*, 3725−3734. (b) Cui, Y.; Yue, Y.; Qian, G.; Chen, B. *Chem. Rev.* **2012**, *112*, 1126−1162. (c) Kreno, L. E.; Leong, K.; Farha, O. K.; Allendorf, M.; Van Duyne, R. P.; Hupp, J. T. *Chem. Rev.* **2012**, *112*, 1105−1125. (d) Hu, Z.; Deibert, B. J.; Li, J. *Chem. Soc. Rev.* **2014**, *43*, 5815−5840.
(9) (a) Lin, W.; Rieter, W. J.; Taylor, K. M. *Angew. Chem., Int. Ed.* **2009**, *48*, 650−658. (b) Horcajada, P.; Chalati, T.; Serre, C.; Gillet, B.; Sebrie, C.; Baati, T.; Eubank, J. F.; Heurtaux, D.; Clayette, P.; Kreuz, C.; Chang, J. S.; Hwang, Y. K.; Marsaud, V.; Bories, P. N.; Cynober, L.; Gil, S.; Férey, G.; Couvreur, P.; Gref, R. *Nat. Mater.* **2010**, *9*, 172−178. (c) Lu, K.; He, C.; Lin, W. *J. Am. Chem. Soc.* **2014**, *136*, 16712−16715.
(10) (a) Ma, L.; Abney, C.; Lin, W. *Chem. Soc. Rev.* **2009**, *38*, 1248−1256. (b) Lee, J.; Farha, O. K.; Roberts, J.; Scheidt, K. A.; Nguyen, S. T.; Hupp, J. T. *Chem. Soc. Rev.* **2009**, *38*, 1450−1459. (c) Yoon, M.; Srirambalaji, R.; Kim, K. *Chem. Rev.* **2012**, *112*, 1196−1231. (d) Liu, J.; Chen, L.; Cui, H.; Zhang, J.; Zhang, L.; Su, C. Y. *Chem. Soc. Rev.* **2014**, *43*, 6011−6061. (e) Dhakshinamoorthy, A.; García, H. *Chem. Soc. Rev.* **2014**, *43*, 5750−5765.
(11) (a) Kataoka, Y.; Sato, K.; Miyazaki, Y.; Masuda, K.; Tanaka, H.; Naito, S.; Mori, W. *Energy Environ. Sci.* **2009**, *2*, 397. (b) Gomes Silva, C.; Luz, I.; Llabrés i Xamena, F. X.; Corma, A.; García, H. *Chem. - Eur. J.* **2010**, *16*, 11133−11138. (c) Horiuchi, Y.; Toyao, T.; Saito, M.; Mochizuki, K.; Iwata, M.; Higashimura, H.; Anpo, M.; Matsuoka, M. *J.*

DOI: 10.1021/acscatal.5b00941
ACS Catal. 2015, 5, 5283−5291

Phys. Chem. C **2012**, *116*, 20848−20853. (d) He, J.; Yan, Z.; Wang, J.; Xie, J.; Jiang, L.; Shi, Y.; Yuan, F.; Yu, F.; Sun, Y. *Chem. Commun.* **2013**, *49*, 6761−6763. (e) Pullen, S.; Fei, H.; Orthaber, A.; Cohen, S. M.; Ott, S. *J. Am. Chem. Soc.* **2013**, *135*, 16997−17003. (f) He, J.; Wang, J.; Chen, Y.; Zhang, J.; Duan, D.; Wang, Y.; Yan, Z. *Chem. Commun.* **2014**, *50*, 7063−7066. (g) Wen, M.; Mori, K.; Kamegawa, T.; Yamashita, H. *Chem. Commun.* **2014**, *50*, 11645−11648. (h) Nasalevich, M. A.; Becker, R.; Ramos-Fernandez, E. V.; Castellanos, S.; Veber, S. L.; Fedin, M. V.; Kapteijn, F.; Reek, J. N. H.; van der Vlugt, J. I.; Gascon, J. *Energy Environ. Sci.* **2015**, *8*, 364−375.

(12) (a) Li, L.; Zhang, S.; Xu, L.; Wang, J.; Shi, L.-X.; Chen, Z.-N.; Hong, M.; Luo, J. *Chem. Sci.* **2014**, *5*, 3808. (b) Wang, D.; Huang, R.; Liu, W.; Sun, D.; Li, Z. *ACS Catal.* **2014**, *4*, 4254−4260.

(13) Nasalevich, M. A.; van der Veen, M.; Kapteijn, F.; Gascon, J. *CrystEngComm* **2014**, *16*, 4919.

(14) (a) Laurier, K. G.; Vermoortele, F.; Ameloot, R.; De Vos, D. E.; Hofkens, J.; Roeffaers, M. B. *J. Am. Chem. Soc.* **2013**, *135*, 14488−14491. (b) Wang, C.-C.; Li, J.-R.; Lv, X.-L.; Zhang, Y.-Q.; Guo, G. *Energy Environ. Sci.* **2014**, *7*, 2831.

(15) (a) Long, J.; Wang, S.; Ding, Z.; Wang, S.; Zhou, Y.; Huang, L.; Wang, X. *Chem. Commun.* **2012**, *48*, 11656−11658. (b) Nasalevich, M. A.; Goesten, M. G.; Savenije, T. J.; Kapteijn, F.; Gascon, J. *Chem. Commun.* **2013**, *49*, 10575−10577. (c) Sun, D.; Ye, L.; Li, Z. *Appl. Catal., B* **2015**, *164*, 428−432.

(16) (a) Wang, C.; deKrafft, K. E.; Lin, W. *J. Am. Chem. Soc.* **2012**, *134*, 7211−7214. (b) Zhou, T.; Du, Y.; Borgna, A.; Hong, J.; Wang, Y.; Han, J.; Zhang, W.; Xu, R. *Energy Environ. Sci.* **2013**, *6*, 3229. (c) Toyao, T.; Saito, M.; Dohshi, S.; Mochizuki, K.; Iwata, M.; Higashimura, H.; Horiuchi, Y.; Matsuoka, M. *Chem. Commun.* **2014**, *50*, 6779−6781.

(17) Wang, C.; Xie, Z.; deKrafft, K. E.; Lin, W. *J. Am. Chem. Soc.* **2011**, *133*, 13445−13454.

(18) Wu, P.; He, C.; Wang, J.; Peng, X.; Li, X.; An, Y.; Duan, C. *J. Am. Chem. Soc.* **2012**, *134*, 14991−14999.

(19) *The Porphyrin Handbook*; Acedemic Press: San Diego, CA, 1999; Vol. *8*.

(20) (a) Feng, D.; Gu, Z. Y.; Li, J. R.; Jiang, H. L.; Wei, Z.; Zhou, H. C. *Angew. Chem., Int. Ed.* **2012**, *51*, 10307−10310. (b) Morris, W.; Volosskiy, B.; Demir, S.; Gándara, F.; McGrier, P. L.; Furukawa, H.; Cascio, D.; Stoddart, J. F.; Yaghi, O. M. *Inorg. Chem.* **2012**, *51*, 6443−6445. (c) Son, H. J.; Jin, S.; Patwardhan, S.; Wezenberg, S. J.; Jeong, N. C.; So, M.; Wilmer, C. E.; Sarjeant, A. A.; Schatz, G. C.; Snurr, R. Q.; Farha, O. K.; Wiederrecht, G. P.; Hupp, J. T. *J. Am. Chem. Soc.* **2013**, *135*, 862−869. (d) Jin, S.; Son, H. J.; Farha, O. K.; Wiederrecht, G. P.; Hupp, J. T. *J. Am. Chem. Soc.* **2013**, *135*, 955−958. (e) Gao, W. Y.; Chrzanowski, M.; Ma, S. *Chem. Soc. Rev.* **2014**, *43*, 5841−5866. (f) Zhao, M.; Ou, S.; Wu, C. D. *Acc. Chem. Res.* **2014**, *47*, 1199−1207. (g) Johnson, J. A.; Lin, Q.; Wu, L. C.; Obaidi, N.; Olson, Z. L.; Reeson, T. C.; Chen, Y. S.; Zhang, J. *Chem. Commun.* **2013**, *49*, 2828−2830. (h) Johnson, J. A.; Chen, S.; Reeson, T. C.; Chen, Y. S.; Zeng, X. C.; Zhang, J. *Chem. - Eur. J.* **2014**, *20*, 7632−7637.

(21) (a) Xie, M. H.; Yang, X. L.; Zou, C.; Wu, C. D. *Inorg. Chem.* **2011**, *50*, 5318−5320. (b) Johnson, J. A.; Zhang, X.; Reeson, T. C.; Chen, Y. S.; Zhang, J. *J. Am. Chem. Soc.* **2014**, *136*, 15881−15884.

(22) (a) Fateeva, A.; Chater, P. A.; Ireland, C. P.; Tahir, A. A.; Khimyak, Y. Z.; Wiper, P. V.; Darwent, J. R.; Rosseinsky, M. J. *Angew. Chem., Int. Ed.* **2012**, *51*, 7440−7444. (b) Sasan, K.; Lin, Q.; Mao, C.; Feng, P. *Chem. Commun.* **2014**, *50*, 10390−10393.

(23) (a) Moghadam, M.; Tangestaninejad, S.; Mirkhani, V.; Mohammadpoor-Baltork, I.; Taghavi, S. A. *J. Mol. Catal. A: Chem.* **2007**, *274*, 217−223. (b) Feng, D.; Gu, Z. Y.; Chen, Y. P.; Park, J.; Wei, Z.; Sun, Y.; Bosch, M.; Yuan, S.; Zhou, H. C. *J. Am. Chem. Soc.* **2014**, *136*, 17714−17717.

(24) Arnold, D. P.; Bartley, J. P. *Inorg. Chem.* **1994**, *33*, 1486−1490.

(25) Williams, R. E. *Science* **1968**, *161*, 276−277.

(26) (a) Sun, J.; Weng, L.; Zhou, Y.; Chen, J.; Chen, Z.; Liu, Z.; Zhao, D. *Angew. Chem., Int. Ed.* **2002**, *41*, 4471−4473. (b) Zhang, J.; Chen, S.; Bu, X. *Angew. Chem., Int. Ed.* **2008**, *47*, 5434−5437. (c) Yang, S.; Lin, X.; Blake, A. J.; Walker, G. S.; Hubberstey, P.; Champness, N. R.; Schröder, M. *Nat. Chem.* **2009**, *1*, 487−493. (d) Xue, Y.-S.; He, Y.; Zhou, L.; Chen, F.-J.; Xu, Y.; Du, H.-B.; You, X.-Z.; Chen, B. *J. Mater. Chem. A* **2013**, *1*, 4525−4530.

(27) Bhatti, M.; Bhatti, W.; Mast, E. *Inorg. Nucl. Chem. Lett.* **1972**, *8*, 133−137.

(28) Eaton, S. S.; Eaton, G. R. *J. Am. Chem. Soc.* **1975**, *97*, 3660−3666.

(29) Arnold, D. P. *Polyhedron* **1986**, *5*, 1957−1963.

(30) Kadish, K. M.; Xu, Q. Y. Y.; Maiya, G. B.; Barbe, J.-M.; Guilard, R. *J. Chem. Soc., Dalton Trans.* **1989**, 1531.

(31) It is noted that the intensity of Q(0,0) around 590−600 nm in emission spectra is significantly diminished in UNLPF-10b, -11, and -12. Also, weak shoulder peaks at ∼ 710 nm appear for UNLPF-10b and -11. These observations, however, should not be attributed to the presence of free-base porphyrin linker for the following reasons. First, no characteristic absorption peak of free base porphyrin at 656 nm was observed (Figure 2). Second, upon acid digestion, both ^{1}H NMR (Supporting Information, Figure S4) and fluorescence emission spectra (Figure S13) of the UNLPF-10b and -11 exhibit no characteristic chemical shift and emissions that correspond to free-base porphyrin moiety, repsectively.

(32) Kadish, K. M.; Morrison, M. M. *J. Am. Chem. Soc.* **1976**, *98*, 3326−3328.

(33) Kadish, K. M.; Cornillon, J. L.; Cocolios, P.; Tabard, A.; Guilard, R. *Inorg. Chem.* **1985**, *24*, 3645−3649.

(34) Cornillon, J. L.; Anderson, J. E.; Kadish, K. M. *Inorg. Chem.* **1986**, *25*, 2611−2617.

(35) Ou, Z.; E, W.; Zhu, W.; Thordarson, P.; Sintic, P. J.; Crossley, M. J.; Kadish, K. M. *Inorg. Chem.* **2007**, *46*, 10840−10849.

(36) (a) Zou, Y. Q.; Chen, J. R.; Liu, X. P.; Lu, L. Q.; Davis, R. L.; Jørgensen, K. A.; Xiao, W. J. *Angew. Chem., Int. Ed.* **2012**, *51*, 784−788. (b) Huang, L.; Cui, X.; Therrien, B.; Zhao, J. *Chem. - Eur. J.* **2013**, *19*, 17472−17482. (c) Pitre, S. P.; McTiernan, C. D.; Ismaili, H.; Scaiano, J. C. *J. Am. Chem. Soc.* **2013**, *135*, 13286−13289.

(37) Mann, C. K.; Barnes, K. K. *Electrochemical Reactions in Nonaqueous Systems*; Marcel Dekker: New York, 1970.

(38) Vasudevan, D.; Wendt, H. *J. Electroanal. Chem.* **1995**, *392*, 69−74.

(39) Franco, C.; Olmsted Iii, J. *Talanta* **1990**, *37*, 905−909.

(40) Gnanaprakasam, B.; Zhang, J.; Milstein, D. *Angew. Chem., Int. Ed.* **2010**, *49*, 1468−1471.

(41) (a) Lang, X.; Ji, H.; Chen, C.; Ma, W.; Zhao, J. *Angew. Chem., Int. Ed.* **2011**, *50*, 3934−3937. (b) Su, F.; Mathew, S. C.; Möhlmann, L.; Antonietti, M.; Wang, X.; Blechert, S. *Angew. Chem., Int. Ed.* **2011**, *50*, 657−660. (c) Park, J. H.; Ko, K. C.; Kim, E.; Park, N.; Ko, J. H.; Ryu, D. H.; Ahn, T. K.; Lee, J. Y.; Son, S. U. *Org. Lett.* **2012**, *14*, 5502−5505.

(42) (a) Berlicka, A.; König, B. *Photochem. Photobiol. Sci.* **2010**, *9*, 1359−1366. (b) Huang, L.; Zhao, J.; Guo, S.; Zhang, C.; Ma, J. *J. Org. Chem.* **2013**, *78*, 5627−5637.

(43) Hurst, J. R.; McDonald, J. D.; Schuster, G. B. *J. Am. Chem. Soc.* **1982**, *104*, 2065−2067.

(44) Rueping, M.; Vila, C.; Koenigs, R. M.; Poscharny, K.; Fabry, D. C. *Chem. Commun.* **2011**, *47*, 2360−2362.

DOI: 10.1021/acscatal.5b00941
ACS Catal. 2015, 5, 5283−5291